1 **Modelling long term Enhanced *in situ* Biodenitrification and induced**

2 **heterogeneity in column experiments under different feeding strategies**

3 Paula Rodríguez-Escales[1,2*], Albert Folch[1,3], Boris M. van Breukelen[4], Georgina Vidal-Gavilan[2,5], Xavier

4 Sanchez-Vila[1]

5 [1]Hydrogeology Group (GHS), Department of Civil and Environmental Engineering, Universitat Politècnica

6 de Catalunya (UPC), c/Jordi Girona 1-3, 08034 Barcelona, Spain.

7 [2]d D'ENGINY biorem S.L., C. Madrazo 68, 08006 Barcelona, Spain.

8 [3]Institut de Ciència i Tecnologia Ambientals (ICTA), Universitat Autònoma de Barcelona (UAB), Bellaterra,

9 Barcelona 08193, Spain

10 [4]Department of Water management, Faculty of Civil Engineering and Geosciences, Delft University of

11 Technology, Stevinweg 1, Delft, The Netherlands.

12 [5]Grup de Mineralogia Aplicada i Geoquímica de Fluïds, Departament de Cristal·lografia, Mineralogia i

13 Dipòsits Minerals, Facultat de Geologia, Universitat de Barcelona, Martí Franquès s/n, 08028, Barcelona,

14 Spain.

15 ***Corresponding author:** paula.rodriguez.escales@upc.edu

16

17

18

19   **Abstract**

20   Enhanced *In situ* Biodenitrification (EIB) is a capable technology for nitrate removal in

21   subsurface water resources. Optimizing the performance of EIB implies devising an

22   appropriate feeding strategy involving two design parameters: carbon injection frequency

23   and C:N ratio of the organic substrate nitrate mixture. Here we model data on the spatial

24   and temporal evolution of nitrate (up to 1.2 mM), organic carbon (ethanol), and biomass

25   measured during a 342 day-long laboratory column experiment (published in Vidal-Gavilan

26   et al., 2014). Effective porosity was 3% lower and dispersivity had a seven-fold increase at

27   the end of the experiment as compared to those at the beginning. These changes in transport

28   parameters were attributed to the development of a biofilm. A reactive transport model

29   explored the EIB performance in response to daily and weekly feeding strategies. The latter

30   resulted in significant temporal variation in nitrate and ethanol concentrations at the outlet

31   of the column. On the contrary, a daily feeding strategy resulted in quite stable and low

32   concentrations at the outlet and complete denitrification. At intermediate times (six months

33   of experiment), it was possible to reduce the carbon load and consequently the C:N ratio

34   (from 2.5 to 1), partly because biomass decay acted as endogenous carbon to respiration,

35   keeping the denitrification rates, and partly due to the induced dispersivity caused by the

36   well-developed biofilm, resulting in enhancement of mixing between the ethanol and nitrate

37   and the corresponding improvement of denitrification rates. The inclusion of a dual-domain

38   model improved the fit at the last days of the experiment as well as in the tracer test

39   performed at day 342, demonstrating a potential transition to anomalous transport that may

40   be caused by the development of biofilm. This modeling work is a step forward to devising

41   optimal injection conditions and substrate rates to enhance EIB performance by minimizing

42   the overall supply of electron donor, and thus the cost of the remediation strategy.

43

1   Introduction

Nitrate is a priority environmental pollutant in many countries due to the combination of high toxicity and widespread presence (European Environment Agency, 2007; Organisation for Economic Co-operation and Development, 2008). Agricultural leaching has been identified as the primary source of groundwater nitrate contamination (Böhlke, 2002; Jahangir et al., 2012). Additional sources of nitrate pollution include landfill leachate, leaking septic tanks, and municipal storm water runoff (Hiscock et al., 1991; Panno et al., 2008).

Different options to reduce the high nitrate concentration levels in groundwater are available, including improved farming practices, delineation of aquifer protection zones, or dilution with low-nitrate water sources. However, these options are seldom available due to legal, logistic, or economical constraints. Thus, groundwater remediation technologies, such as ion exchange, reverse osmosis, electrodialysis, and Enhanced *in situ* Biodenitrification (EIB) (Haugen et al., 2002), are often the only practical options left to deal with nitrate-contaminated aquifers.

EIB holds environmental and economic advantages over the other remediation methods mentioned, because it is simple, selective, and cost efficient (Smith et al., 2001). The technology is based on the reduction of nitrate to dinitrogen gas by anaerobic heterotrophic facultative bacteria that use nitrate as electron acceptor. Such bacteria are ubiquitous in soil and groundwater (Beauchamp et al., 1989). EIB is feasible anywhere bacteria may thrive, organic electron donors can be supplied, and oxygen levels are below 1-2 mg/L (Korom, 1992). In natural aquifer conditions, a major limiting factor for

66   biodenitrification is organic matter. Therefore, the main idea behind EIB is the addition of

67   an organic carbon source (acting as electron donor for nitrate reduction and as a carbon

68   source for biomass growth), while controlling a suite of environmental parameters such as

69   the concentrations of other oxidants (e.g. O_2), pH, and nutrient levels (e.g. phosphorous or

70   oligo-elements). Optimal configuration of EIB, involving the presence of one or more

71   injection and extraction wells, is site specific, depending on pumping rate, groundwater

72   flow velocity, and residence time of nitrate in the system (Khan and Spalding, 2004).

73   The injection of organic carbon during EIB creates a bioactive zone, characterized

74   by the growth of denitrifier biomass, heterogeneously distributed throughout the porous

75   media depending on nutrient availability. Biomass can be found either as suspended matter

76   or as biofilms attached to the solid matrix. Biofilms occur as micro-colonies or aggregates

77   composed by denitrifier microorganisms, extracellular polymeric or proteinic substances

78   (EPS), and potentially trapped dinitrogen gas formed during denitrification (Dupin and

79   McCarty, 2000; Hand et al., 2008; Rittmann, 1993; Vandevivere and Baveye, 1992).

80   As biofilm develops and the pore space is occupied, partial bioclogging might take

81   place, affecting a number of hydraulic properties. In addition to bioclogging, a reduction of

82   hydraulic conductivity can be associated with the presence of trapped N_2 gas (Amos and

83   Mayer, 2006; Jarsjö and Destouni, 2000). While the word clogging is traditionally defined

84   in terms of the overall reduction in hydraulic conductivity (Vandevivere and Baveye,

85   1992), the decrease in effective pore volume caused by biofilm growth also changes

86   porosity. Due to the variation of these two hydraulic parameters, changes in groundwater

87   velocity might be recorded (Pavelic et al., 2007; Taylor and Jaffé, 1990; Taylor et al.,

88   1990), changing residence time between injection and extraction wells, thus influencing the

5

overall capacity for biodenitrification. Furthermore, the spatial heterogeneity of hydraulic properties caused by the inhomogeneous distribution of biofilm throughout the porous media also promotes changes in dispersivity (Seifert and Engesgaard, 2007). Dispersivity is an important parameter as it affects the mixing of nitrate with injected organic substrate, and it is sometimes the limiting factor for the reaction processes (Dentz et al., 2011).

Thus, the amount of biomass and the way it grows significantly affect the performance of EIB facilities. Biomass growth is driven among other things by the feeding strategy, i.e., the frequency of injection, the total carbon supplied, and the resulting carbon-nitrogen ratio (C:N). With the objective of limiting the biomass growth, some authors suggested injecting the electron donor in discrete pulses rather than as a continuous supply (Franzen et al., 1997; Gierczak et al., 2007; Peyton, 1996; Semprini et al., 1991; Semprini et al., 1990; Shouche et al.). Nevertheless, little is known about how the frequency of injection pulses affects biomass growth and nitrate degradation. Regarding the C:N ratio, Vidal-Gavilan et al. (2014) observed that even working with low C:N ratios (C:N=1; below the stoichiometric one: C:N = 2.5), high denitrification rates were achieved after biofilm development. The authors attributed this to the occurrence of endogenous bacterial decay.

Proper understanding of processes occurring during EIB involves the need for multispecies reactive transport modeling (RTM) (Chen and MacQuarrie, 2004; Lee et al., 2006; Rodríguez-Escales et al., 2016). Such models can facilitate exploring a variety of remediation strategies such as injection duration and rate, and concentration of reactants. Nevertheless, there is a need to develop specific models to evaluate how different feeding strategies interact with transport processes.

111   The present work is aimed at developing a model capable of reproducing different

112   feeding injection frequencies (from weekly to daily) with different C:N ratios in a long term

113   column experiment of Enhanced *in situ* Biodenitrification, lasting 342 days (Vidal-Gavilan

114   et al., 2014). This modeling study focusses on the EIB performance in response to the

115   frequency of organic substrate addition as well as the changes in hydraulic and transport

116   properties promoted by the growth of biofilm. Proper understanding of the processes taking

117   place allow defining the optimal injection strategy (frequency and rate) capable of

118   enhancing EIB performance (high performance at low cost) by minimizing the overall

119   supply of labile organic carbon substrate.

120   **2   Materials and Methods**

121   **2.1   Description of the experiment and data set**

122   A full description of the experiment is provided in Vidal-Gavilan et al. (2014), and

123   sketched here in Figure 1 for completeness. It consisted of a glass cylindrical column (70

124   cm length, 8 cm inner diameter) filled with unconsolidated sediment from a sandy alluvial

125   aquifer (located in Argentona, NE Spain). The sediment was composed by medium and

126   coarse-grained sand mainly made up of quartz and feldspar and with a small silt content,

127   the organic matter content in the sediment was negligible (Vidal-Gavilan et al., 2014).

128   Water was forced to flow from the bottom to the top of the column with a pump-controlled

129   average flow-rate of 180 mL/d resulting in a residence time in the column of about 6.4

130   days. A total of eight sampling ports were installed: one at the inflow reservoir, six along

131   the column (at 6, 16, 26, 36, 46 and 56 cm from inlet), and one at the outflow, allowing the

132   delineation of aqueous compounds and suspended biomass profiles at different predefined

133   times. The data set provided in Vidal-Gavilan et al. (2014) and used in the modeling effort

134   includes aqueous concentrations of ethanol, nitrate, and biomass at selected times at the

135   sampling ports placed within the column. A control experiment without carbon substrate

136   addition ran for 2 months, and natural denitrification was not observed, as changes in

137   nitrate along the column were lower than 1% (Vidal-Gavilan et al., 2014).

138   The water used in the experiment was obtained from an existing large-diameter well

139   located at the site. Three 25-L containers were used to store the input water for the

140   experiment, filled up at different days (August 2011, December 2011, and April 2012). The

141   well was always purged prior to sampling. No forced deoxygenation took place, so that the

142   input water (see Table 1) was oxic and saturated with oxygen. The experiment ran for 342

143   days at aquifer temperature (15ºC). Ethanol was added as an external organic carbon source

144   by means of four injectors located 16 cm from the inlet (see Figure 1). It was added by

145   mixing it with the input water previous to injection (Table 1). Different feeding strategies

146   were tested during the experiments (Table 2), characterized by different injection

147   frequencies (weekly *versus* daily) and carbon to nitrogen molar ratios (from 2.5 to 1). In

148   this ratio the amount of C is computed from the concentration of ethanol multiplied with

149   the duration of injection (0.5 min). Feeding was twice discontinued, first between days 150

150   and 175 due to pump failure (no water was supplied), and then between days 286 and 311,

151   this time to evaluate the resilience of the system to the absence of feeding (water with no

152   ethanol was supplied during that second period).

153   Two tracer tests were performed, one previous to the start of the experiment, before

154   any feeding took place, and a second one at day 342. The tests were conducted under

155   continuous flow with constant concentration of bromide (1.45 and 2.23 mM, respectively).

156   During the two tracer tests the flow rate was 835 mL/d. The bromide breakthrough curves

157   were monitored at the outflow point.

2.2   Model construction

159   Here we describe first the biogeochemical equations used in the biodenitrification model;

160   second, the hydrogeological parameters derived from the two tracer tests; third, the codes

161   used in the modeling effort; and fourth, the calibration process.

2.2.1   EIB biogeochemical model

163   Biodenitrification was modelled considering both nitrate respiration and biomass growth

164   (see e.g., Rodríguez-Escales et al., 2014). The reactions considered are:

$$165 \qquad r_{ED} = -k_{max} \frac{[ED]}{[ED]+K_{S,ED}} \frac{[EA]}{[EA]+K_{S,EA}} [X] \tag{1}$$

$$166 \qquad r_{EA} = Qr_{ED} - Sb[X] \tag{2}$$

$$167 \qquad r_X = -Y_h r_{ED} - b[X] \tag{3}$$

168   where [ED] is the concentration of the electron donor (ethanol, C_2H_5OH); [EA] that of the

169   electron acceptor (nitrate), and [X] the denitrifier biomass concentration, all expressed in

170     $[ML^{-3}]$; k_{max} $[T^{-1}]$ is the consumption rate of electron donor per unit value of biomass; $K_{S,ED}$

171     $[ML^{-3}]$ and $K_{S,EA}$ $[ML^{-3}]$ the half saturation constants of electron donor and acceptor,

172   respectively; b $[T^{-1}]$ a biomass decay constant; Y_h the microbial yield [C biomass / C

173   ethanol], and Q [N nitrate / C ethanol] and S [N nitrate / C endogenous]. Both K_{max}

174   (μ_{max}/Y_h) and K_s were fitting parameters, whereas S and Q were stoichiometric factors

175   determined by the driving denitrification reaction (4). Biomass was conceptualized as

176   having an average chemical composition of $C_5H_7O_2N$ (Porges et al., 1956).

177          $0.943\ C_2H_5OH + 1\ NO_3^- + 0.489\ H^+ = 0.273\ C_5H_7O_2N + 0.364\ N_2 + 0.511\ HCO_3^- + 1.864\ H_2O$ (4)
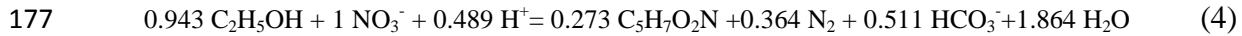
178   Equation (4) was determined following the instructions of Rittmann and McCarty (2001)

179   and it applies to the following determined parameter values: (i) the portion of substrate

180   (ethanol) used for cell synthesis during denitrification (Y_h) was 0.724 C-biomass/C-ethanol

181   (in agreement with Rodríguez-Escales et al. 2014); and (ii) the portion of nitrate consumed

182   by substrate oxidation (Q) was 0.53 mol nitrate-mol C-ethanol. The stoichiometric

183   relationship between nitrate and endogenous carbon (S) was 0.92 mol nitrate-mol C

184   endogenous, following (Rodríguez-Escales et al., 2014).

185   Although the injected solution was partly to almost fully oxic (oxygen concentrations

186   measured varied between 0.06 and 0.2 mM), ethanol oxidation by oxygen was and could be

187   neglected. This assumption was based on ethanol consumption by oxygen being between

188   0.1 and 4% of ethanol injected (depending on initial concentrations). Moreover, preliminary

189   models considering instantaneous reduction of oxygen showed that oxygen was consumed

190   within the first 5 cm of the column (results not shown). Considering all of this and in order

191   to simplify the model, ethanol oxidation by oxygen was not contemplated.

192   Nitrite accumulation was not relevant in the experiment (only present during the first

193   20 d, in concentrations below 0.1 mM; whereas nitrate decreased then with 1.2-1.6 mM.).

194   Therefore, the model contemplates only one step reduction from nitrate to dinitrogen gas.

195   The potential accumulation of NO and N_2O was discarded because the system was

196   maintained at low oxygen concentrations, with enough labile organic carbon, and with pH

197 values between 7 and 8; under these conditions complete denitrification is expected (Rivett

198 et al., 2008; Tallec et al., 2008).

199   Most often, the amount of bacteria suspended in the aqueous phase is quite small as

200 compared to that attached to the aquifer matrix (Barry et al., 2002; Rittmann, 1993). As a

201 way to implement a practical model, minimizing the number of fitting parameters, we

202 assumed that all biomass was attached to the solid matrix, and thus immobile, without

203 considering attachment and detachment processes, described for example in Clement et al.

204 (1997). The initial biomass concentration was estimated in 6.5 x 10^{-8} mmol/kg, considering

205 a most probable number for denitrifying cells equal to 37.5 cel/ml (Vidal-Gavilan et al.

206 2014) and converted to moles using a denitrifier cell weight of 10^{-9} mg (Alvarez et al.,

207 1994). The initial value used in PHT3D was normalized by liter of water.

208   Finally, the column was considered as an open system in equilibrium with the

209 atmosphere because it was open at its upper part. Thus, degassing was allowed if the sum of

210 partial pressures of gases (mainly dinitrogen gas and carbon dioxide) exceeded the

211 atmospheric pressure. Prior to the simulation process, and in order to evaluate the potential

212 hydraulic conductivity variations due to bubble formation, we evaluated the potential

213 building up of denitrification gases. Thus, we ran the model under closed system

214 conditions. The results showed that the hydrostatic pressure was exceeded in most feeding

215 strategies illustrating that degassing could occur. To limit the chance for gas entrapment,

216 which would be the main responsible of changes in hydraulic conductivity (Amos and

217 Mayer, 2006), we purposely ran the column experiment in vertical mode with water

218 flowing upwards. In this way, gas entrapment should have been limited as any gas formed

219 could escape at the top outlet of the column and the flow of gas bubbles and water in the

220   column were aligned. Furthermore, we expect that the coarse sand (grain size between 1

221   and 2 mm) used in the column further limited any gas entrapment.

2.2.2   Transport model parameters evaluated from the tracer tests

223   Two tracer tests with a conservative tracer (Br-) were performed at days 0 and 342 in order

224   to build a conceptual model for conservative transport and to estimate the corresponding

225   hydraulic parameters. Invoking the parsimony principle, we first tried to fit the

226   breakthrough curves with the simplest model, that of the one-dimensional advection-

227   dispersion equation (ADE).

228   The ADE model could properly reproduce the test performed at time 0, but failed to

229   fit the tail of the experimental BTC obtained during the second test at day 342. As an

230   alternative model we selected a dual porosity model (Delay et al., 2013; Haggerty and

231   Gorelick, 1995; Lawrence et al., 2002; Seifert and Engesgaard, 2007), representing the

232   porous medium as composed of a mobile and of an immobile region that coexist at any

233   given point in the domain. The first one was an aqueous phase where advection and

234   dispersion were the main transport processes, whereas the second one was a (diffusion zone

235   governed by biofilm dynamics). Both regions exchange mass proportionally to the

236   difference in their concentrations at any given time. The equation describing the

237   concentration of species i in the mobile zone, $c_{m,i}$, is:

$$\phi_m \frac{\partial C_{m,i}}{\partial t} = -q \frac{\partial C_{m,i}}{\partial x} + \phi_m \frac{D \partial^2 C_{m,i}}{\partial x^2} - \Gamma_i \qquad (5)$$

239   where D is the dispersion coefficient, q is Darcy's velocity, ϕ_m the porosity corresponding

240   to the mobile zone (aqueous phase with aqueous solution), and Γ_i the source-sink term

241 controlling the mass transfer of species i between the mobile (m) and the immobile regions

242 (im) (biofilm phase with microorganisms attached to the sediment), given by:

243
$$\Gamma_i = \alpha\phi_{im}\left(C_{m,i} - C_{im,i}\right) \tag{6}$$

244 with α the mass transfer rate $[T^{-1}]$, ϕ_{im} [-] the porosity associated with the immobile region

245 (volume fraction occupied by the biofilm), and $C_{im,i}$ the concentration of species i in the

246 immobile region. The actual total porosity is $\phi_t = \phi_m + \phi_{im}$, and remains constant during

247 biofilm formation. The rationale behind it is that the biofilm colonizes pores that were

248 initially occupied by water in sediments not affected by consolidation or swelling, so that

249 the sediment occupied the same volume at the beginning and end of the experiment. A key

250 parameter characterizing the shape of the BTC in the dual porosity model is the ratio of

251 porosities (Fernàndez-Garcia and Sanchez-Vila, 2015) given by:

252
$$\beta = \frac{\phi_{im}}{\phi_m} = \frac{\phi_t}{\phi_m} - 1 \tag{7}$$

253 **2.2.3 Used codes and calibration process**

254 The PHT3D model code (v. 2.17) (Prommer and Post, 2010) was used to simulate the

255 evolution of groundwater hydrochemistry during enhanced biodenitrification in the column.

256 This model couples the transport simulator MT3DMS (Zheng and Wang, 1999) and the

257 geochemical model PHREEQC-2 (Parkhurst and Appelo, 1999), by means of a sequential

258 split-operator technique. Regarding solute transport, PHT3D incorporates either the

259 traditional ADE, or else the dual domain model through MT3DMS. Since the PHT3D

260 reaction module uses the original PHREEQC-2 database syntax, equilibrium and non-

261 equilibrium reaction chains can be defined. For reactions in equilibrium, the constants were

262 taken directly from the database. Kinetic reactions such as ethanol degradation and

263 bacterial growth/decay (1-3), not being part of the standard database, were incorporated

264 into the module in the form of BASIC routines, as explained in Rodríguez-Escales et al.

265 (2014) and Carrey et al. (2014).

266   Regarding the tracer tests, the interpretation using the traditional ADE and the dual

267 domain model was carried out with the CXTFIT code (Toride et al., 1999). We developed

268 the inverse modelling of transport processes using the experimental information of the

269 BTCs from the tracer tests and we determined the following parameters: dispersivity

270 coefficient, total, mobile and immobile porosities, and, dual domain transfer coefficient.

271 Furthermore, CTXFIT provides the confidence interval (95%) of each parameter as well as

272 their corresponding standard deviations. In order to avoid the correlation between immobile

273 porosity and dispersivity coefficient in the transport equation (e.g. Wehrer et al. 2012), the

274 calibration process was divided in two steps. First of all, we calibrated the dispersivity

275 coefficient and the mobile porosity without considering the tail. Then, we incorporated the

276 dual domain model to improve the fittings of the tail, allowing an independent estimation of

277 the immobile porosity. Following this methodology, we only related the dispersivity to the

278 change into the geometry and not also to the diffusion processes avoiding its correlation

279 with immobile porosity.

280   To assist the biodenitrification model calibration process, the model independent

281 parameter estimation program PEST (Doherty, 2005) was coupled to PHT3D and used to

282 estimate the reaction rate parameters ($k_{max,}$ $K_{S,ED,}$ $K_{S,EA}$, and b). PEST computed the

283 sensitivities, correlations, and linear uncertainties (confidence intervals) of the optimized

284 model parameters. For the calibration process, the error associated with the measurement

285 was treated as 95% confidence interval, and weights were applied using the inverse of the

286 standard deviation of this confidence interval (Karlsen et al., 2012). Using this method,

287 values with a higher accuracy get assigned a higher weight and the resulting objective

288 function became dimensionless. Standard ranges for measurement error of chemical

289 sampling were given with an accuracy of 5%. Weights (w) for each chemical species

290 observation i were thus calculated:

291
$$w_i = \frac{1.96}{\varepsilon_i C_i} \tag{8}$$

292 where ε is the measurement error described above and C is the observed concentration. For

293 the calibration process, we used the experimental data of nitrate during the first 100 days of

294 the experiment (35 points). The calibration process of the reactive transport was performed

295 by fixing the conservative transport parameters. Finally, we also evaluated the likelihood of

296 the models comparing the Akaike information criterion values (AIC) calculated by PEST.

297 **3   Results and discussion**

298 **3.1   Tracer tests interpretation: derivation of transport processes and parameters**

299 The first step is the interpretation of the 1-D conservative tracer tests. The traditional ADE

300 equation was capable of properly fitting the curve corresponding to the first test, but it

301 failed to provide a good fit of the tail of the BTC corresponding to the second test, with a

302 maximum error in estimated concentrations of 3%. On the other hand, the dual domain

303 model was capable to reproduce the tail of the BTC corresponding to the second test

304 indicating a transition from a Fickian description of transport at the start to an anomalous

305 description of transport at the end of the EIB experiment. The reported BTCs are presented

15

306   in Figure 2, together with the best fits obtained either with code CTXFIT at day 0 (single

307   porosity) and at day 342 (dual porosity); the fitted parameters are listed in Table 3.

308   Groundwater velocity was very similar in the two tests (see Table 3). The hydraulic

309   gradient could not be measured in the applied experimental setup. Therefore, any reduction

310   in hydraulic conductivity due to biofilm growth could not be assessed. Total (single-phase)

311   porosity and dispersivity were estimated from the first test; total porosity, the proportion of

312   immobile and mobile porosity, dispersivity, and the mass transfer rate were estimated from

313   the second one. Total porosity values estimated from both tests were statistically not

314   different, with best estimates of 0.33±0.03 to 0.34±0.05, and estimation intervals largely

315   overlapping (Table 3). However, the dual porosity model estimated an immobile porosity of

316   0.015±0.009 at day 342.

317   There was a remarkable seven-fold increase in the dispersivity coefficient estimated

318   from the two tests, with the mean value changing from 0.48±0.01 to 3.44±0.25 cm (see

319   Table 3). This result is consistent with the observations by Taylor and Jaffé (1990) who

320   also described an increase in immobile porosity linked to an increase in dispersivity in a

321   column experiment colonized by biomass. Several studies also report significant changes in

322   dispersivity, ranging from two- to eight-fold increases, in bioremediation experiments

323   lasting 2-7 weeks (Arnon et al., 2005; Bielefeldt et al., 2002; Hill and Sleep, 2002; Seifert

324   and Engesgaard, 2007; Sharp et al., 1999; Taylor and Jaffé, 1990; Taylor et al., 1990), and

325   as high as a 10-100 fold variation for long duration experiments (Taylor and Jaffé, 1990;

326   Bielefeldt et al., 2002). This increase in dispersivity is generally associated to denitrifier

327   biomass colonizing the sand grains forming the soil skeleton. Thus, while total porosity

328   remained basically constant, a small fraction was colonized by biomass aggregates and

329 micro-colonies, changing its behavior from water accessible by flow (mobile) to

330 inaccessible (immobile). Such aggregates have been reported to induce irregular surfaces of

331 the solid particles (Rittmann, 1993), and consequently, to increase the heterogeneity in the

332 pore size distribution (Seifert and Engesgaard, 2007), thus enhancing dispersivity.

333   The change in the conceptual model of transport was associated with the growth of

334 biofilm during the duration of the experiment. Thus, the fitted parameters of the dual

335 domain model have a clear physical explanation; for example, the calibrated α parameter (α

336 $= 0.019\pm0.018$ d^{-1}) can be interpreted as the inverse of the characteristic diffusive time of

337 bromide transport through the immobile phase (thus being equal to 45 days). Moreover, the

338 β value ($\beta = 0.046\pm0.030$) represented the proportion of the void volume occupied by the

339 biofilm (4.65 ± 2.96 %).

340   Regarding the calibration process of the transport parameters, the automatic

341 calibration showed that during the two steps of calibration the parameters were not

342 correlated because the correlation coefficients were lower than 0.95 (Hill et al., 1998).

343 During the first step (calibration using ADE of velocity and dispersion), the correlation

344 among parameters was lower than 0.025 for the two tracer tests. During the second step, the

345 correlation between immobile porosity and the mass transfer coefficient was 0.21. The

346 coefficients of variation (CV) of the parameters of ADE were well estimated, as their

347 values were generally low (less than 0.15). Regarding the parameters of the dual domain

348 model, they were estimated as highly uncertain.

3.2 Long-term modeling of EIB. Impact of organic carbon injection strategies

Based on tracer tests results the column experiment was first interpreted using a Fickian representation of transport, i.e., based on the ADE. Emphasis was placed on the performance of the daily and weekly feeding strategies upon the observed temporal evolution of the concentrations of nitrate, ethanol, and biomass. Since Table 3 displays two dispersivity values corresponding to days 0 and 342, but no intermediate values were obtained, the 342-day column experiment was modeled using both dispersivity values, by assuming that they lasted the full duration of the experiment, thus providing two limiting cases. The column was discretized into 70 elements of 1 cm length. The time discretization was selected to satisfy Peclet and Courant criteria. Dispersive transport was computed by the third-order Total Variation Diminishing solution, a feature available in PHT3D.

The actual data and the fittings with the two dispersivity values are shown in Figure 3. Neither porosity (obtained from the tracer test, 0.33), nor the geochemical parameters of reactions in equilibria (selected from the PHREEQC2 database) were calibrated. The only calibrated parameters were the microbiological ones (Table 4) and, all were in range compared to values reported in the literature. Note that the we compared the μ_{max} parameter instead the k_{max} with literature values, because it only depends on velocity reaction and it is easier to compare. The automatic calibration procedure used for the estimation of kinetic parameters in the denitrification model showed that the evaluated parameters were not cross-correlated, as indicated by their values in the coefficient correlation matrix being below 0.747 (data not shown). That is, given the available observations for model calibration, each model parameter affected the simulated equivalents to the observations sufficiently differently. The values of the coefficients of variation, CVs, were relatively

18

372   high, ranging from 0.26 to 0.61. As pointed out by Greskowiak et al. (2005), large CVs do

373   not necessarily imply an incorrect model concept. Instead, it may indicate that the available

374   observation data are insufficient to uniquely constrain (estimate) the parameter, or that

375   there is an underlying physical basis for relatively high CVs.

376   The lowest dispersivity value (0.48 cm) resulted in a good fitting of the experimental

377   data during the weekly feeding strategy (Figure 3), lasting the first 98 days, indicating that

378   during this period dispersivity did not change significantly. This result is in contrast with

379   other works based on column experiments using somewhat different experimental

380   conditions like organic substrate but were all fed continuously (Bielefeldt et al., 2002;

381   Seifert and Engesgaard, 2007; Taylor and Jaffé, 1990) (Table 5). For example, Seifert and

382   Engesgaard (2007), using acetate and oxygen as electron acceptor, reported an increase in

383   dispersivity from 0.33 cm to 1.1 cm in 64 days. On the other hand, Bielefeldt et al. (2002),

384   in an experiment on propylene glycol degradation using nitrate as electron acceptor,

385   observed a 20-60 fold increase in 15 days in clean sand. Finally, Delay et al. (2013)

386   reported a noticeable change in dispersivity in a 1.4 day column denitrification experiment.

387   In short, from the data in Table 5, it seems that a weekly feeding strategy limits dispersivity

388   increases with time.

389   We note that Figure 4 reports the modeling results assuming a constant representative

390   dispersivity value all throughout the column. We expect though that most of the biomass

391   colonization took place around the injection point (Kildsgaard and Engesgaard, 2001),

392   associated with the highest EA and ED concentrations and, consequently, the modification

393   of the transport parameters too. Although the general trends were well captured, the

394   limitation of considering only one set of transport parameters could explain the

395   discrepancies between the experimental data and the simulated results.

396   During the daily feeding strategy, starting after day 99, the best overall fit of nitrate

397   concentration was obtained with the final dispersivity value of 3.43 cm. This is visible both

398   for time-series (Figure 3) and for spatial profiles (Figure 4). Consequently, the increase in

399   dispersivity seems triggered by the changes in feeding strategy, from weekly to daily

400   pulses. During weekly injection, biomass was not fed homogenously, and probably biomass

401   growth was through colonies or aggregates that did not colonizing the whole sandy media.

402   On the other hand, daily injection drove a more continuous growth of biomass (probably in

403   biofilm form) and favoring the colonization of the whole column (Rittmann, 1993). We

404   thus contend that induced heterogeneity was larger in the daily scenario as compared to the

405   weekly one, and consequently, a seven-fold increase of dispersivity in the former feeding

406   strategy was observed. This increase was smaller than others reported in the literature for

407   continuous feeding (see Table 5 for values and references). This can be explained because

408   the injection was performed in the form of a daily pulse, rather than fully continuous.

409   Besides this change in feeding strategy, the two stop periods in daily feeding strategies

410   could also facilitate the increasing of heterogeneity due to the detachment of biomass and

411   its redistribution through the column (Wehrer et al., 2012). This suggests that both the

412   feeding frequency and the stop periods are key operational parameters that may affect

413   hydraulic parameters and thereby control the transport of chemical species during EIB.

414   We want to emphasize that the increase of dispersivity was evaluated in a column

415   experiment (1D), thus only considering longitudinal dispersivity. Although it is still

416   unknown how biofilm growth will disturb the dispersivity in 3-D (e.g. field applications),

417   we would expect an increase in the three directions of dispersivity, longitudinal, and

418   transversal both horizontally and vertically. The last two of those having a most significant

419   impact upon the enhancement of spreading and mixing of nutrients (Chiogna et al., 2012;

420   Rolle et al., 2009).

421   The biomass concentration decreased corresponding to the low C:N ratios (Figure 3).

422   Note that the biomass concentration did not differ between feeding strategies I and II,

423   indicating that the injection frequency played a lower role than the C:N ratio. Nevertheless,

424   we hypothesize that the biomass growth was different for each strategy. Whereas during

425   weekly feeding strategy, the biomass distribution should not be continuous, in the daily one

426   we should expect that a connected biofilm was formed. This idea follows the observations

427   of Rittmann (1993), who determined that a continuous feeding causes a biofilm whereas a

428   discontinued   one   resulted   in   disconnected   biomass   aggregates.   Although   the

429   characterization of the attached biomass could be done at the end of the experiment (e.g.

430   Clement et al. (1997)), we recommend for future research the characterization of the

431   biofilm structure through SEM (Scanning Electron Microscope) images.

432   **3.3   The implication of introducing non-Fickianity in the conceptual model**

433   The incorporation of a dual domain transport model resulted in a slight improvement of the

434   model fit from day 183 onwards (Figure 3 and 4, blue dashed-dotted line). The parameters

435   used in the model are reported in Table 3 for transport processes (last row) and Table 4 for

436   the biogeochemical ones. Note that the mass transfer coefficient had a high standard

437   deviation (0.019) in relation to the parameter value (0.018). Considering that, we run the

438 model with different mass transfer values. The results showed that the model was not very

439 sensitive to this change (results not shown).

440 As the fit obtained during the weekly feeding strategy by ADE was quite good, much

441 better than the obtained with the non-Fickian model (Figure 3), we contend that during this

442 period the diffusive transport through the biofilm was negligible. Thus, the

443 conceptualization of the porous medium as a dual domain was not considered until the daily

444 feeding strategy started, that supposed to enhance the biofilm developing (conceptualized

445 as immobile porosity). This improvement in fitting is attributed to modeling the partial

446 transformation of initial pores to non-flowing volume (immobile porosity or diffusive

447 layer) that act as electron donor sink. Yet, it is still unknown at which point of the

448 experiment this process was relevant. This could only be assessed by the incorporation of

449 non-invasive techniques to monitor biofilm evolution in future studies. We emphasize that

450 water velocity conditioned the significance of involving a dual domain into the conceptual

451 transport model. Thus, the impact of a dual domain model in the tracer test interpretation

452 (Figure 2) was more significant than that on the biodenitrification experiment (Figure 3-4)

453 because the water velocity was higher (0.5 m/d instead of 0.1 m/d) and thus the time

454 available for mass transfer between the domain was less. Although this difference in

455 velocity, we want to remark that the dual domain model was more likely than the ADE

456 model because its AIC value was the lowest one (203.22 compared to 212.55).

457 **3.4 Significance of the C:N ratio and implications for EIB design**

458 In the scenarios with the lowest C:N ratios (strategies III, days 206-252 and IV, days 253-

459 342), the model correctly reproduces the experimental data of nitrate and ethanol being

460   completely consumed inside the column (not detected at the outlet). This means that the

461   source of organic carbon was used optimally, fully consumed, as opposed to that observed

462   in strategy I. Note that the increase in dispersivity resulted in enhanced spreading and then

463   mixing of the injected ethanol with nitrate, enabling a more efficient substrate use.

464   Another parameter that helped defining the success of the different injection

465   strategies is the stress produced upon the biomass population. When the carbon load was

466   reduced (strategies III and IV), the modeled biomass diminished (see Figure 3). However,

467   nitrate remained undetected, indicating that denitrification was partially linked to biomass

468   decay (endogenous respiration) meaning that there was not enough external carbon to

469   maintain the large biomass population (see Figure 5). The use of endogenic carbon as

470   electron donor in bioremediation facilities has already been reported in other works

471   (Béranger et al., 2006; Rodríguez-Escales et al., 2016). The decrease in biomass

472   concentration indicated that the low C:N strategies were not sustainable in time.

473   Nevertheless, working with low C:N could be a good tool to reduce the risk of clogging.

474   Besides this, the amount of ethanol used in these strategies was lower than in

475   strategies I and II (Figure 6), which would imply important savings (the main cost in an

476   EIB operation is electron donor injection). A proper design of the amount of carbon

477   supplied could represent significant savings in an EIB technology. For these reasons, we

478   recommend applying low C:N strategies when the system has reached maturity (complete

479   denitrification achieved, mature biofilm, no nitrite accumulation) and/or when an important

480   risk of clogging exists (monitored with continuous or semi continuous measurement of

481   hydraulic conductivity and mobile porosity).

4   Summary and conclusions

An Enhanced *In situ* Biodenitrification experiment, performed in a 70 cm long column under virtually constant flow rate and different feeding strategies was modeled. Injection strategies were defined in terms of periodicity of injection of organic carbon (ethanol), and thus resulting C:N ratio. A long term reactive transport (342 d) model based on the Advection Dispersion Equation (ADE) fitted properly most of the experimental data.

Throughout the experiment, estimated dispersivity varied from the beginning to the end of the experiment. During the weekly supply strategy I (first 98 days), the best fit was obtained using a low dispersivity value (0.48 cm), whereas during the daily strategy, it was best fitted with a larger dispersivity value (3.43 cm). We attributed this increase to the change in injection periodicity, from weekly to daily, after day 98, resulting in biofilm growth. Furthermore, after day 252, with a very mature system, data fitted better using a dual-domain model (i.e., non-Fickian) as compared to one based on the ADE. This change was associated with the presence of a diffusive layer (biofilm) increasing its relevance with time. Although the dynamic conditions of the system, the presented model has been capable of reproducing satisfactorily the experimental observations in all feeding strategies.

On the other hand, reducing the C:N ratio below the stoichiometric requirements allowed the optimization of ethanol injection into the system avoiding its presence at the column outlet. At this point, biomass decay increased and the endogenous carbon acted as partial source of electron donor during the denitrification process. Nevertheless, the decrease of modelled biomass concentration in time showed that this strategy is not

503 sustainable at long term and that it only can be used when a mature biofilm exists in the

504 subsurface.

505 Our work has shown that besides other parameters (nutrient loading, flow rate, or grain

506 size), injection frequency is a significant operational parameter that can affect a number of

507 hydraulic parameters, notably dispersivity. This finding could be extended to promote field

508 Enhanced *In Situ* Biodenitrification (EIB) applications. A larger dispersivity value offers

509 the possibility of enhancing spreading of injected solutes, increasing the area treated per

510 injection point and limiting the organic carbon loss in this particular *in situ* technique. Thus,

511 this will promote the growth of biofilm and, when a mature system is eventually reached,

512 reducing the C:N ratio can minimize the risk of clogging. So, in order to improve efficiency

513 and saving costs in real field scale applications, feeding strategy in terms of frequency and

514 C:N relationship should be evaluated before the design and construction of EIB

515 installations, as well as during its operation.

516 **Acknowledgements**

523

524 **References**

525 Alvarez, P., Anid, P., Vogel, T., 1994. Kinetics of Toluene Degradation by Denitrifying Aquifer

526   Microorganisms. J. Environ. Eng., 120(5): 1327-1336. DOI:10.1061/(ASCE)0733-

527   9372(1994)120:5(1327)

528 Amos, R.T., Mayer, K.U., 2006. Investigating the role of gas bubble formation and entrapment in

529   contaminated aquifers: Reactive transport modelling. J. Contam. Hydrol., 87(1–2): 123-154.

530   DOI:http://dx.doi.org/10.1016/j.jconhyd.2006.04.008

531 Arnon, S., Adar, E., Ronen, Z., Yakirevich, A., Nativ, R., 2005. Impact of microbial activity on the

532   hydraulic properties of fractured chalk. J. Contam. Hydrol., 76(3-4): 315-36.

533   DOI:10.1016/j.jconhyd.2004.11.004

534 Barry, D.A. et al., 2002. Modelling the fate of oxidisable organic contaminants in groundwater.

535   Adv. Water Resour., 25(8–12): 945-983. DOI:10.1016/S0309-1708(02)00044-1

536 Beauchamp, E.G., Trevors, J.T., Paul, J.W., 1989. Carbon Sources for Bacterial Denitrification. In:

537   Stewart, B.A. (Ed.), Adv. Soil. Sci. Springer New York, pp. 113-142. DOI:10.1007/978-1-

538   4613-8847-0_3

539 Bielefeldt, A., McEachern, C., Illangasekare, T., 2002. Hydrodynamic Changes in Sand due to

540   Biogrowth on Naphthalene and Decane. J. Environ. Eng., 128(1): 51-59.

541   DOI:10.1061/(ASCE)0733-9372(2002)128:1(51)

542 Béranger, S., Sleep, B., Sherwood Lollar, B., Brown, A., 2006. Isotopic Fractionation of

543   Tetrachloroethene Undergoing Biodegradation Supported by Endogenous Decay. J.

544   Environ. Eng., 132(7): 725-735. DOI:10.1061/(ASCE)0733-9372(2006)132:7(725)

545 Böhlke, J.-K., 2002. Groundwater recharge and agricultural contamination. Hydrogeol. J., 10(1):

546   153-179. DOI:10.1007/s10040-001-0183-3

547 Carrey, R. et al., 2014. Nitrate attenuation potential of hypersaline lake sediments in central Spain:

548   Flow-through and batch experiments. J. Contam. Hydrol., 164(0): 323-337.

549   DOI:http://dx.doi.org/10.1016/j.jconhyd.2014.06.017

550 Chen, D.J.Z., MacQuarrie, K.T.B., 2004. Numerical simulation of organic carbon, nitrate, and

551   nitrogen isotope behavior during denitrification in a riparian zone. J. Hydrol., 293(1–4):

552   235-254. DOI:10.1016/j.jhydrol.2004.02.002

553 Chiogna, G., Hochstetler, D.L., Bellin, A., Kitanidis, P.K., Rolle, M., 2012. Mixing, entropy and

554   reactive solute transport. Geophysical Research Letters, 39(20): L20405.

555   DOI:10.1029/2012GL053295

556 Clement, T.P., Peyton, B.M., Skeen, R.S., Jennings, D.A., Petersen, J.N., 1997. Microbial growth

557   and transport in porous media under denitrification conditions: experiments and

558   simulations. J. Contam. Hydrol., 24(3–4): 269-285. DOI:http://dx.doi.org/10.1016/S0169-

559   7722(96)00014-9

560 Delay, F., Porel, G., Chatelier, M., 2013. A dual flowing continuum approach to model

561   denitrification experiments in porous media colonized by biofilms. J. Contam. Hydrol.,

562   150(0): 12-24. DOI:http://dx.doi.org/10.1016/j.jconhyd.2013.04.001

563 Dentz, M., Le Borgne, T., Englert, A., Bijeljic, B., 2011. Mixing, spreading and reaction in

564   heterogeneous media: A brief review. J. Contam. Hydrol., 120–121(0): 1-17.

565   DOI:http://dx.doi.org/10.1016/j.jconhyd.2010.05.002

566 Doherty, J., 2005. PEST: model independent parameter estimation. Watermark Numerical

567   Computing, fifth edition of user manual.

568 Dupin, H.J., McCarty, P.L., 2000. Impact of Colony Morphologies and Disinfection on Biological

569   Clogging in Porous Media. Environ. Sci. Technol., 34(8): 1513-1520.

570   DOI:10.1021/es990452f

571 European Environment Agency, E., 2007. Present concentration of nitrate in groundwater bodies in

572   European countries, 2003.

573   Fernàndez-Garcia, D., Sanchez-Vila, X., 2015. Mathematical equivalence between time-dependent

574   single-rate and multirate mass transfer models. Water Resour. Res., 51(5): 3166-3180.

575   DOI:10.1002/2014WR016348

576   Franzen, M.E.L., Petersen, J.N., Clement, T.P., Hooker, B.S., Skeen, R.S., 1997. Pulsing of

577   multiple nutrients as a strategy to achieve large biologically active zones during in situ

578   carbon tetrachloride remediation. Comput. Geosci., 1(3): 271-288.

579   DOI:10.1023/A:1011573429996

580   Gierczak, R., Devlin, J.F., Rudolph, D.L., 2007. Field test of a cross-injection scheme for

581   stimulating in situ denitrification near a municipal water supply well. J. Contam. Hydrol.,

582   89(1–2): 48-70. DOI:http://dx.doi.org/10.1016/j.jconhyd.2006.08.001

583   Greskowiak, J., Prommer, H., Vanderzalm, J., Pavelic, P., Dillon, P., 2005. Modeling of carbon

584   cycling and biogeochemical changes during injection and recovery of reclaimed water at

585   Bolivar, South Australia. Water Resour. Res., 41(10): W10418.

586   DOI:10.1029/2005WR004095

587   Haggerty, R., Gorelick, S., 1995. Multiple-Rate Mass Transfer for Modeling Diffusion and Surface

588   Reactions in Media with Pore-Scale Heterogeneity. Water Resour. Res., 31(10): 2383-2400.

589   DOI:10.1029/95WR10583

590   Hand, V.L., Lloyd, J.R., Vaughan, D.J., Wilkins, M.J., Boult, S., 2008. Experimental studies of the

591   influence of grain size, oxygen availability and organic carbon availability on bioclogging

592   in porous media. Environ. Sci. Technol., 42(5): 1485-91.

593   Haugen, K.S., Semmens, M.J., Novak, P.J., 2002. A novel in situ technology for the treatment of

594   nitrate contaminated groundwater. Water Res., 36(14): 3497-3506.

595   DOI:http://dx.doi.org/10.1016/S0043-1354(02)00043-X

596   Hill, D.D., Sleep, B.E., 2002. Effects of biofilm growth on flow and transport through a glass

597   parallel plate fracture. J. Contam. Hydrol., 56(3-4): 227-46.

598   Hill, M.C., Cooley, R.L., Pollock, D.W., 1998. A Controlled Experiment in Ground Water Flow

599   Model Calibration. Ground Water, 36(3): 520-535. DOI:10.1111/j.1745-

600   6584.1998.tb02824.x

601   Hiscock, K.M., Lloyd, J.W., Lerner, D.N., 1991. Review of natural and artificial denitrification of

602   groundwater. Water Res., 25(9): 1099-1111. DOI:http://dx.doi.org/10.1016/0043-

603   1354(91)90203-3

604   Jahangir, M.M.R., Johnston, P., Khalil, M.I., Richards, K.G., 2012. Linking hydrogeochemistry to

605   nitrate abundance in groundwater in agricultural settings in Ireland. J. Hydrol., 448–449:

606   212-222. DOI:http://dx.doi.org/10.1016/j.jhydrol.2012.04.054

607   Jarsjö, J., Destouni, G., 2000. Degassing of deep groundwater in fractured rock around boreholes

608   and drifts. Water Resour. Res., 36(9): 2477-2492. DOI:10.1029/2000WR900131

609   Karlsen, R.H., Smits, F.J.C., Stuyfzand, P.J., Olsthoorn, T.N., van Breukelen, B.M., 2012. A post

610   audit and inverse modeling in reactive transport: 50 years of artificial recharge in the

611   Amsterdam water supply dunes. J. Hydrol., 454–455(0): 7-25.

612   DOI:http://dx.doi.org/10.1016/j.jhydrol.2012.05.019

613   Khan, I.A., Spalding, R.F., 2004. Enhanced in situ denitrification for a municipal well. Water Res.,

614   38(14–15): 3382-3388. DOI:http://dx.doi.org/10.1016/j.watres.2004.04.052

615   Kildsgaard, J., Engesgaard, P., 2001. Numerical analysis of biological clogging in two-dimensional

616   sand box experiments. J. Contam. Hydrol., 50(3–4): 261-285.

617   DOI:http://dx.doi.org/10.1016/S0169-7722(01)00109-7

618   Korom, S.F., 1992. Natural denitrification in the saturated zone: A review. Water Resour. Res.,

619   98(6). DOI:doi:10.1029/92WR00252

620   Lawrence, A.E., Sanchez-Vila, X., Rubin, Y., 2002. Conditional moments of the breakthrough

621   curves of kinetically sorbing solute in heterogeneous porous media using multirate mass

622   transfer models for sorption and desorption. Water Resour. Res., 38(11): 1248.

623   DOI:10.1029/2001WR001006

624 Lee, M.-S., Lee, K.-K., Hyun, Y., Clement, T.P., Hamilton, D., 2006. Nitrogen transformation and

625 transport modeling in groundwater aquifers. Ecol. Modell., 192(1–2): 143-159.

626 DOI:10.1016/j.ecolmodel.2005.07.013

627 Organisation for Economic Co-operation and Development, O., 2008. Environmental performance

628 of agriculture in OECD countries since 1990.

629 Panno, S.V., Kelly, W.R., Hackley, K.C., Hwang, H.-H., Martinsek, A.T., 2008. Sources and fate of

630 nitrate in the Illinois River Basin, Illinois. J. Hydrol., 359(1–2): 174-188.

631 DOI:http://dx.doi.org/10.1016/j.jhydrol.2008.06.027

632 Parkhurst, D.L., Appelo, C.A.J., 1999. User's guide to PHREEQC (version 2) - a computer program

633 for speciation, reaction-path, 1D-transport, and inverse geochemical calculations., U.S.

634 GEOLOGICAL SURVEY.

635 Pavelic, P. et al., 2007. Water quality effects on clogging rates during reclaimed water ASR in a

636 carbonate aquifer. J. Hydrol., 334(1–2): 1-16.

637 DOI:http://dx.doi.org/10.1016/j.jhydrol.2006.08.009

638 Peyton, B.M., 1996. Improved biomass distribution using pulsed injections of electron donor and

639 acceptor. Water Res., 30(3): 756-758. DOI:http://dx.doi.org/10.1016/0043-1354(95)00220-

640 0

641 Porges, N., Jasewicz, L., Hoover, S., 1956. Principles of biological oxidation. In biological

642 treatment of sewage and industrial wastes. Reinhold. Publ., New York.

643 Prommer, H., Post, V., 2010. A Reactive Multicomponent Transport Model for Saturated Porous

644 Media. User's Manual. v2.10.

645 Rittmann, B.E., 1993. The significance of biofilms in porous media. Water Resour. Res., 29(7):

646 2195-2202. DOI:10.1029/93WR00611

647 Rittmann, B.E., McCarty, P.L., 2001. Environmental biotechnology : principles and applications.

648 McGraw-Hill, cop. 2001.

649   Rivett, M.O., Buss, S.R., Morgan, P., Smith, J.W.N., Bemment, C.D., 2008. Nitrate attenuation in

650   groundwater: A review of biogeochemical controlling processes. Water Res., 42(16): 4215-

651   4232. DOI:10.1016/j.watres.2008.07.020

652   Rodríguez-Escales, P., Folch, A., Vidal-Gavilan, G., van Breukelen, B.M., 2016. Modeling

653   biogeochemical processes and isotope fractionation of enhanced in situ biodenitrification in

654   a   fractured   aquifer.   Chem.   Geol.,   425:   52-64.

655   DOI:http://dx.doi.org/10.1016/j.chemgeo.2016.01.019

656   Rodríguez-Escales, P., van Breukelen, B., Vidal-Gavilan, G., Soler, A., Folch, A., 2014. Integrated

657   modeling of biogeochemical reactions and associated isotope fractionations at batch scale:

658   A tool to monitor enhanced biodenitrification applications. Chem. Geol., 365(0): 20-29.

659   DOI:http://dx.doi.org/10.1016/j.chemgeo.2013.12.003

660   Rolle, M., Eberhardt, C., Chiogna, G., Cirpka, O.A., Grathwohl, P., 2009. Enhancement of dilution

661   and transverse reactive mixing in porous media: Experiments and model-based

662   interpretation.   J.   Contam.   Hydrol.,   110(3–4):   130-142.

663   DOI:http://dx.doi.org/10.1016/j.jconhyd.2009.10.003

664   Seifert, D., Engesgaard, P., 2007. Use of tracer tests to investigate changes in flow and transport

665   properties due to bioclogging of porous media. J. Contam. Hydrol., 93(1–4): 58-71.

666   DOI:http://dx.doi.org/10.1016/j.jconhyd.2007.01.014

667   Semprini, L. et al., 1991. In-situ biotransformation of carbon tetrachloride under anoxic conditions.

668   Semprini, L., Roberts, P.V., Hopkins, G.D., McCarty, P.L., 1990. A Field Evaluation of In-Situ

669   Biodegradation of Chlorinated Ethenes: Part 2, Results of Biostimulation and

670   Biotransformation Experiments. Ground Water, 28(5): 715-727. DOI:10.1111/j.1745-

671   6584.1990.tb01987.x

672   Sharp, R.R., Cunningham, A.B., Komlos, J., Billmayer, J., 1999. Observation of thick biofilm

673   accumulation and structure in porous media and corresponding hydrodynamic and mass

transfer effects. Water Sci. Technol., 39(7): 195-201. DOI:http://dx.doi.org/10.1016/S0273-1223(99)00168-7

Shouche, M.J., Petersen, J.N., Skeen, R.S., Use of a mathematical model for prediction of optimum feeding strategies forin situ bioremediation. Appl. Biochem. Biotech., 39(1): 763-779. DOI:10.1007/BF02919034

Smith, R.L., Miller, D.N., Brooks, M.H., Widdowson, M.A., Killingstad, M.W., 2001. In situ stimulation of groundwater denitrification with formate to remediate. Environ. Sci. Technol., 35(1): 196-203.

Tallec, G., Garnier, J., Billen, G., Gousailles, M., 2008. Nitrous oxide emissions from denitrifying activated sludge of urban wastewater treatment plants, under anoxia and low oxygenation. Bioresource Technology, 99(7): 2200-2209. DOI:http://dx.doi.org/10.1016/j.biortech.2007.05.025

Taylor, S.W., Jaffé, P.R., 1990. Biofilm growth and the related changes in the physical properties of a porous medium: 3. Dispersivity and model verification. Water Resour. Res., 26(9): 2171-2180. DOI:10.1029/WR026i009p02171

Taylor, S.W., Milly, P.C.D., Jaffé, P.R., 1990. Biofilm growth and the related changes in the physical properties of a porous medium: 2. Permeability. Water Resour. Res., 26(9): 2161-2169. DOI:10.1029/WR026i009p02161

Toride, N., Leij, F.J., van Genuchten, M.T., 1999. The CXTFIT code for estimating transport parameters from laboratory or field tracer experiments.

Vandevivere, P., Baveye, P., 1992. Saturated Hydraulic Conductivity Reduction Caused by Aerobic Bacteria in Sand Columns. Soil Sci. Soc. Am. J.(1): 1-13.

Vidal-Gavilan, G., Carrey, R., Solanas, A., Soler, A., 2014. Feeding strategies for groundwater enhanced biodenitrification in an alluvial aquifer: Chemical, microbial and isotope assessment of a 1D flow-through experiment. Sci.Total Environ., 494–495(0): 241-251. DOI:http://dx.doi.org/10.1016/j.scitotenv.2014.06.100

700   Wehrer, M., Jaesche, P., Totsche, K.U., 2012. Modeling the kinetics of microbial degradation of

701   deicing chemicals in porous media under flow conditions. Environ. Pollut., 168: 96-106.

702   DOI:http://dx.doi.org/10.1016/j.envpol.2012.04.016

703   Zheng, C., Wang, P.P., 1999. MT3DMS: A modular three-dimensional multispecies model for

704   simulation of advection, dispersion and chemical reactions of contaminants in groundwater

705   systems. Documentation and User's Guide, Contract Reo. SERDP-99-41. U.S. Army Eng.

706   Res. and Dev. Cent., Vicksburg, Miss.

707

Figure captions

708

709   **Figure 1.** Experimental flow-through system and location of the sampling ports.

710   **Figure 2.** Model fits using the ADE (black lines) and a dual domain model (red dashed

711   lines). Square symbols (□) correspond to measurements corresponding to the tracer test

712   performed at day 0 (red and black lines run in top of each other), whereas circles (○)

713   correspond to the BTC from the test at day 342. The error bars are related to the bromide

714   analyses.

715   **Figure 3.** Results of the EIB models considering different injection strategies at the outflow

716   of the column (70 cm). The black and the red solid lines were obtained with dispersivity

717   values of 0.48 and 3.43 cm, respectively, considering an ADE equation. The dashed-dotted

718   blue line corresponds to a model using a dispersivity value of 3.43 cm and a dual model

719   mass transfer. The dashed black line corresponds to ethanol concentration in the injection

720   solution. Grey areas represents the two periods without feeding. The bottom plot shows the

721   simulated biomass concentrations (represented in mM) at the last cell of the model domain

722   (70 cm).

723   **Figure 4.** Nitrate distance profiles (simulated vs. measured) at 12 different times. In each

724   plot, the first number represents the sampling day, and that in brackets reflects the elapsed

725   time since the last injection period. The black and the red dashed lines were obtained with

726   dispersivity values of 0.48 and 3.43 cm, respectively, considering an ADE equation. The

727   blue dashed doted line in the last two plots corresponds to a model using a dispersivity

728   value of 3.43 cm and a dual model mass transfer. The grey zone corresponds to the

729   injection point.

Figure 5. Detail of feeding strategies with low C:N ratio without considering decay of biomass (top line) and biomass decay (bottom line). Filling zone indicates the importance of biomass decay on nitrate consumption rates under low C:N.

Figure 6. Comparison of the amount of ethanol used in injections and percentage of denitrification achieved by the different feeding strategies. The percentage of denitrification was calculated as the difference in nitrate mass between the inlet and the outlet of the column divided by the nitrate mass at the inlet.

Table captions

Table 1. Average concentration of different species in the input water. Nitrate concentration (*) varied during the experiment due to seasonal nitrate oscillations within the aquifer.

Table 2. Summary of the different feeding strategies (I to IV) tested during the experiment, in terms of feeding frequency, ethanol concentration supplied, ratio of C (external organic carbon source concentration) to N (nitrate concentration), and duration.

Table 3. Hydraulic parameters estimated for the two bromide tracer tests. The standard deviation was calculated by using the inverse problem with CTXFIT. The interpretation models were different for the two tests: the initial one (day 0) with an ADE model; the second one (day 342) with the dual domain model, thus involving two additional parameters. The R^2 of two fitted curves were 0.999 and 0.998, respectively.

749   **Table 4.** Biogeochemical constants used in the denitrification model, compared with values

750   compiled from the literature. Both the median and the standard deviation were determined

751   by automatic calibration using PEST.

752   **Table 5.** Comparison between the values obtained in this work and in similar experiments

753   compiled from the literature, including feeding strategies, organic carbon inflow, flow rate

754   and estimated increase in the dispersivity after some period of time.

Figure1
Click here to download high resolution image
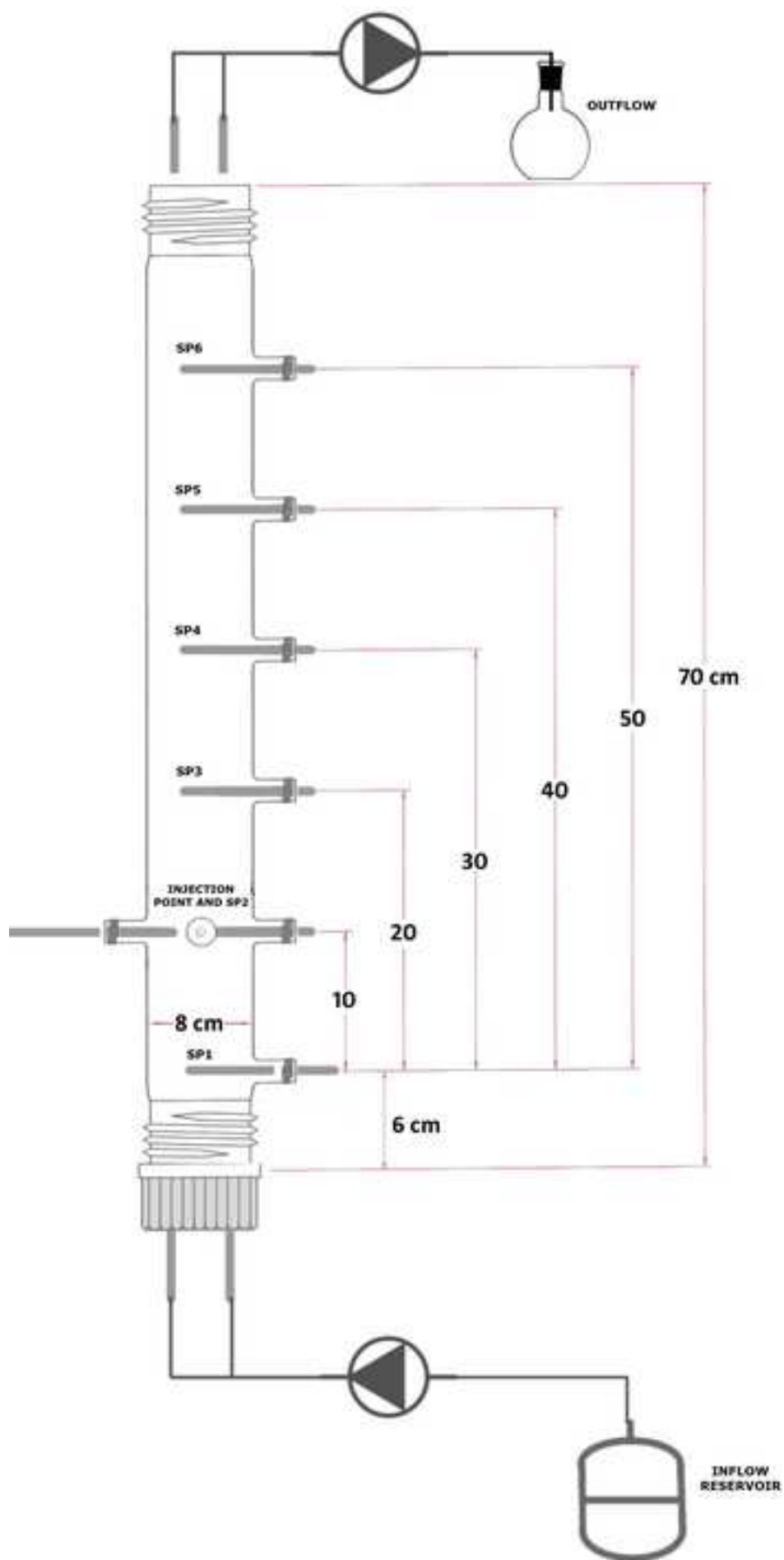
Figure2
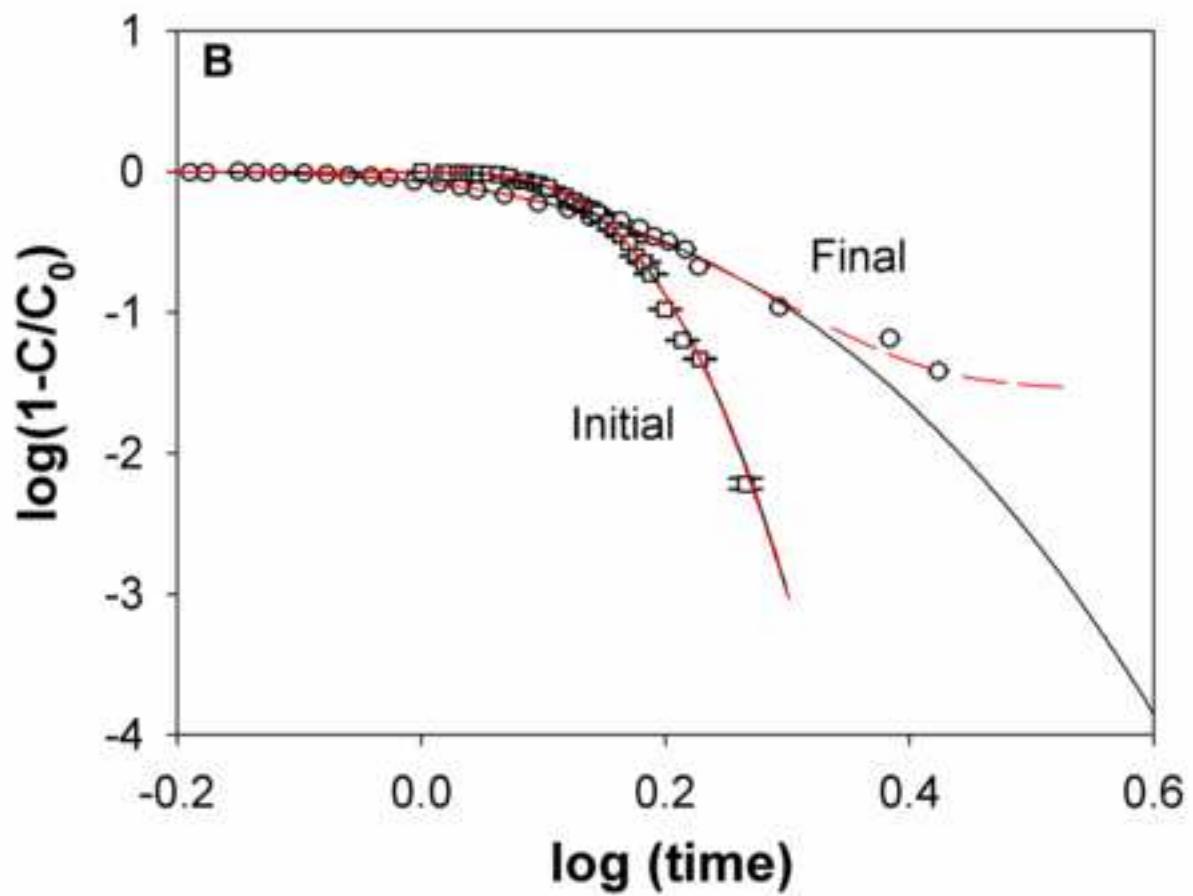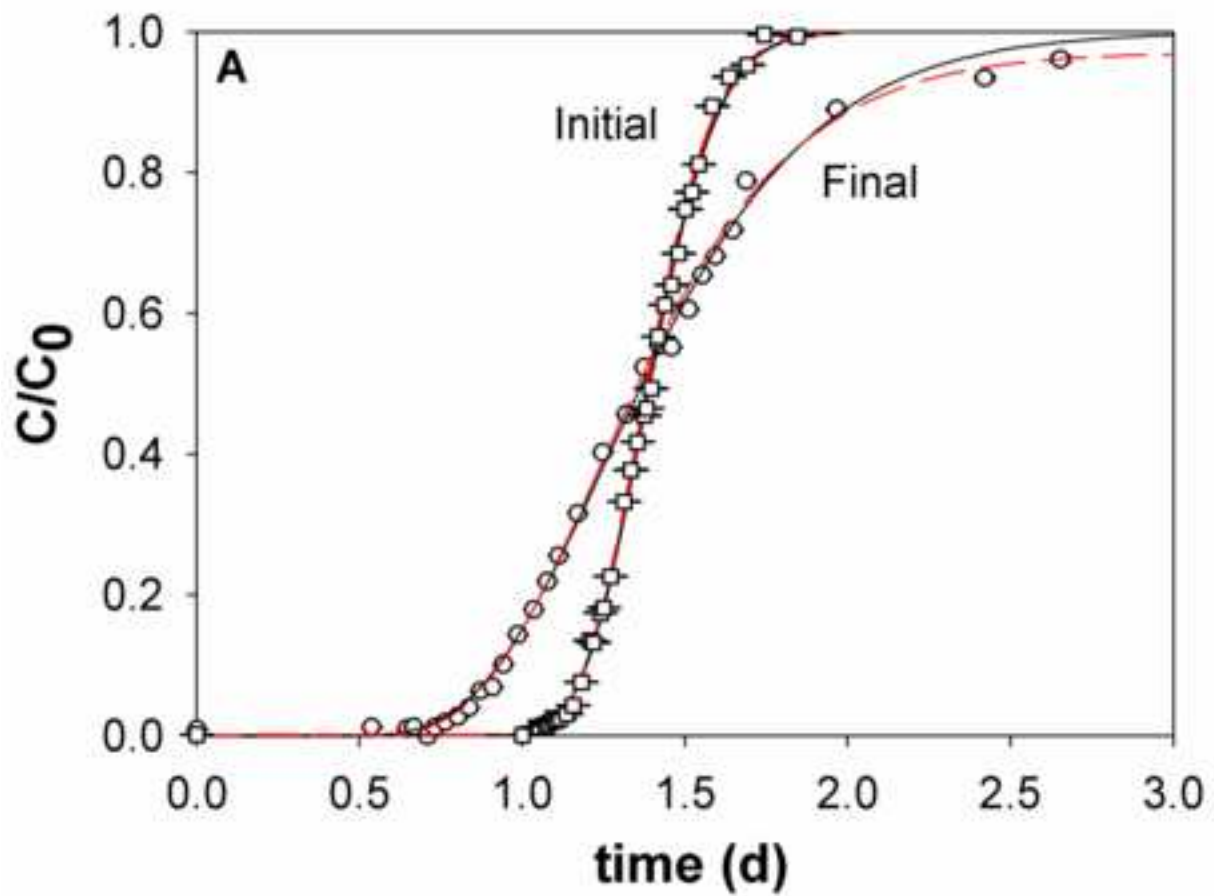**Click here to download high resolution image**
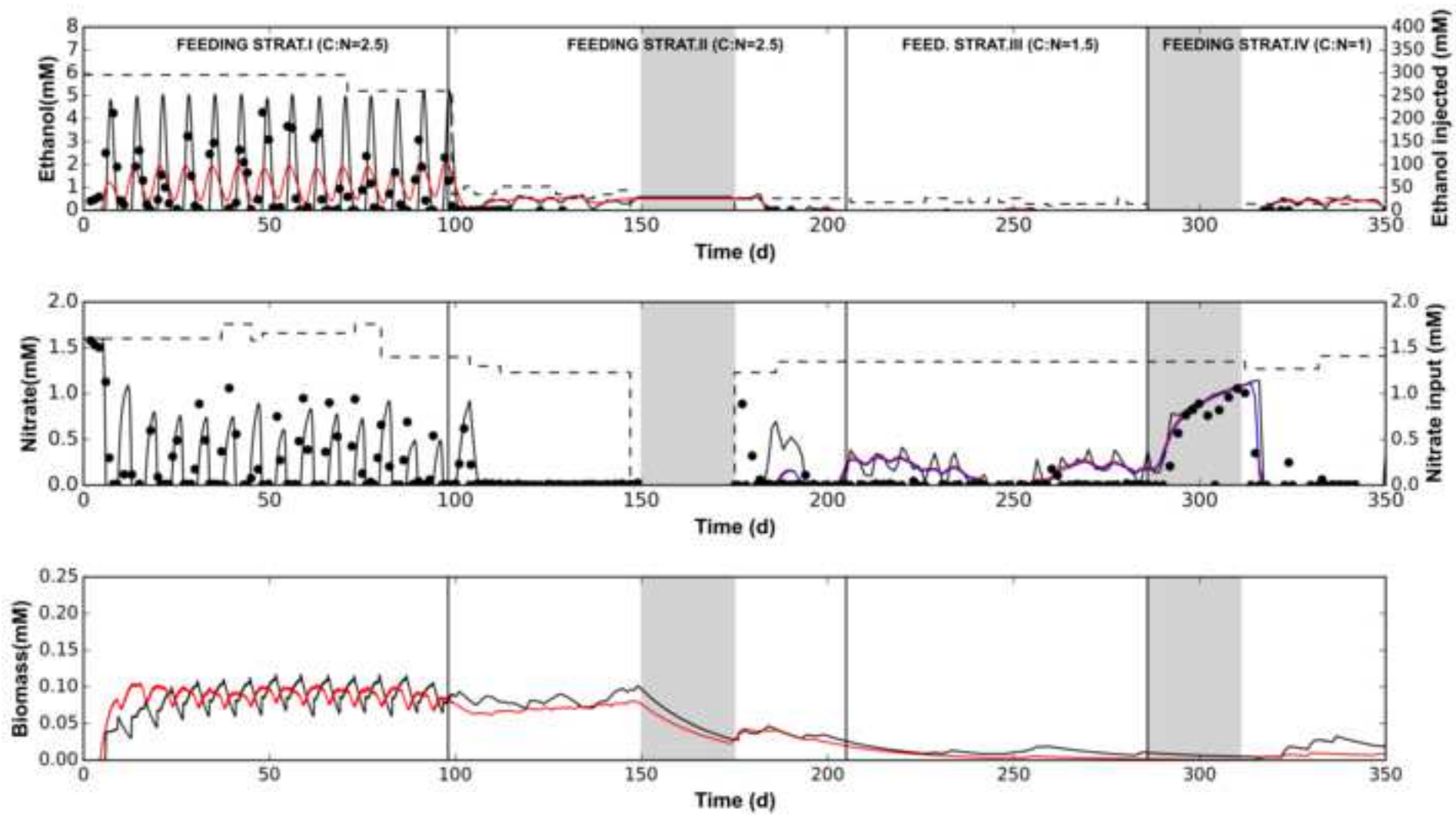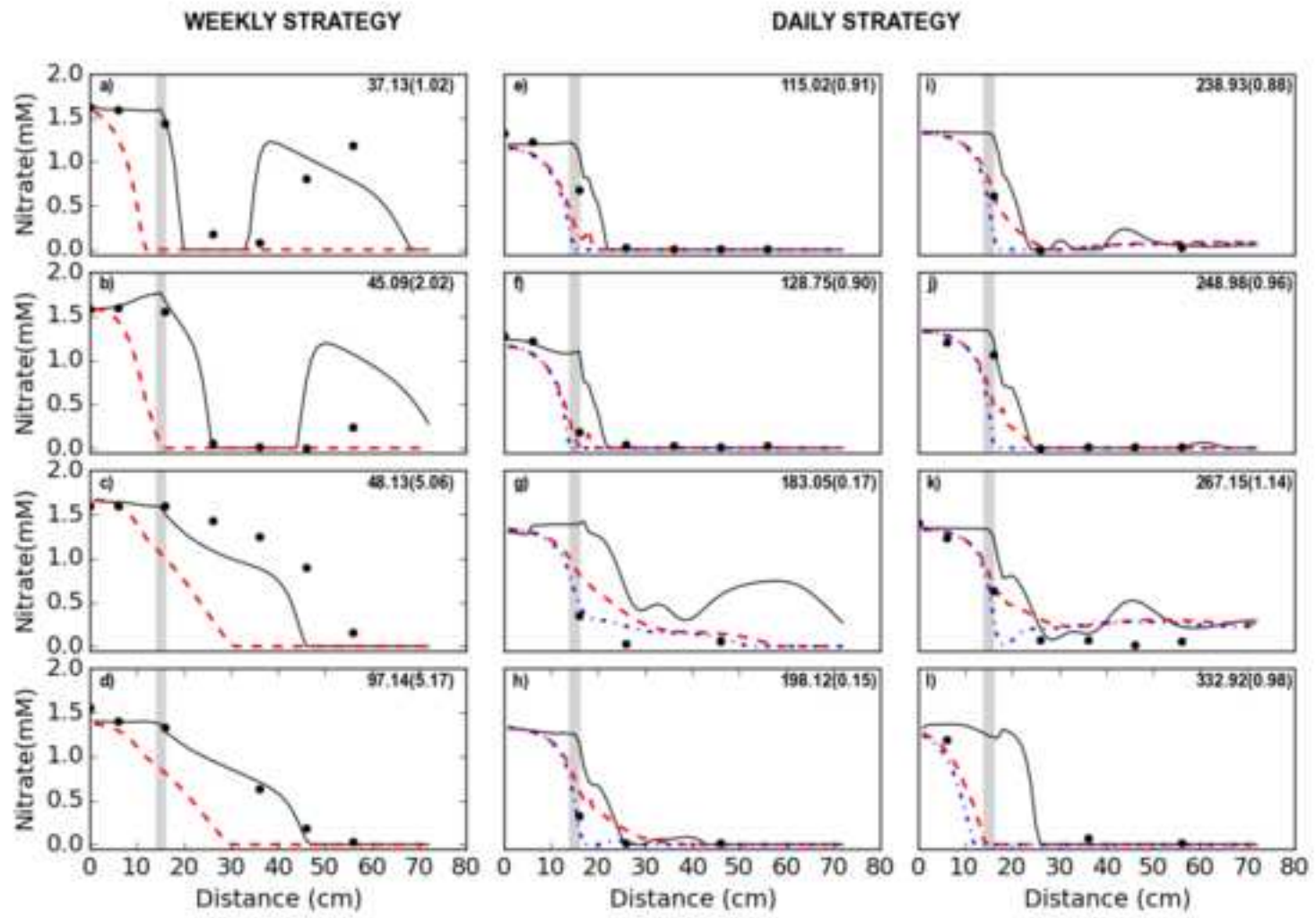
Figure 4

Figure5
Click here to download high resolution image
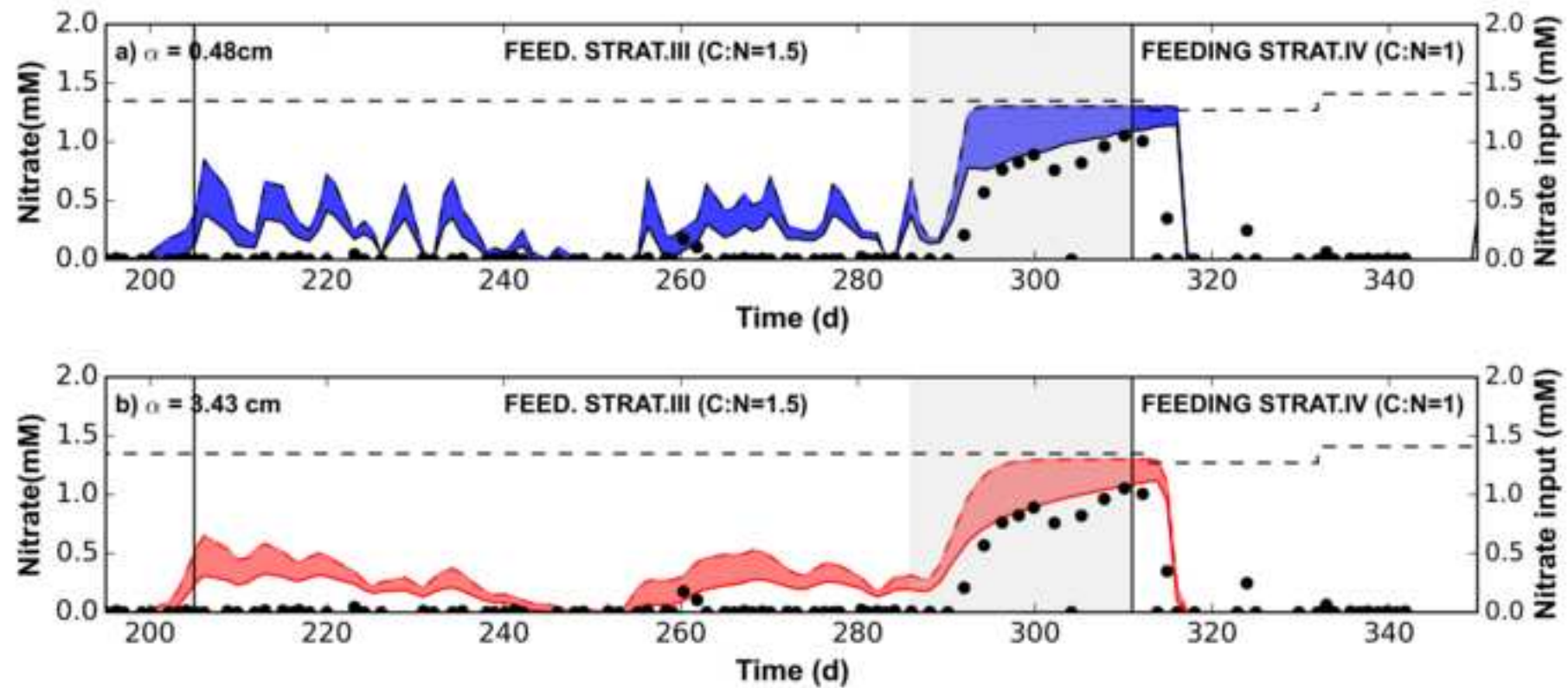
Figure6
Click here to download high resolution image

Table1

Parameter	Unit	Column solution	Injected solution
pH		7.2 ± 0.1	7.2 ± 0.1
Temperature	ºC	15	15
Nitrate	mM	1.2-1.6 (*)	1.2-1.6 (*)
DIC	mM	7.2 ± 1.0	7.2 ± 1.0
Chloride	mM	0.10 ± 0.04	0.10 ± 0.04
Sulfate	mM	1.2 ± 0.1	1.2 ± 0.1
Calcium	mM	3.40 ± 0.07	3.40 ± 0.07
Sodium	mM	2.20 ± 0.04	2.20 ± 0.04
Magnesium	mM	1.60 ± 0.03	1.60 ± 0.03
Potassium	mM	0.100 ± 0.001	0.100 ± 0.001
Ethanol	mM	-	14-292
Biomass	mM	2.3×10^{-7}	

Table2

Feeding strategy	Feeding frequency	Average C:N	Ethanol injected (mM ethanol)	Days of experiment
I	Weekly	2.5	261-292	1-98
II	Daily	2.5	26-35	99-205*
III	Daily	1.5	17	206-287
IV	Daily	1	14	287-342**

*Supply of water was discontinued between days 150 and 175

**Supply of organic carbon was discontinued between days 286 and 311

Table3

	Groundwater velocity (m d^{-1})	MODEL TYPE	Mobile Porosity	Dispersivity (cm)	Mass transfer parameter (α, d^{-1})	Immobile porosity
Initial	0.5036 ± 0.0004	ADE	0.331 ± 0.033	0.485 ± 0.006	N/A	N/A
End	0.5107 ± 0.0018	Dual domain	0.326 ± 0.044	3.440 ± 0.246	0.019± 0.018	0.015 ± 0.009

Parameter	Unit	This work	Literature values	Reference[a]
μ_{max}	$[d^{-1}]$	$3.01 \times 10^1 \pm 1.82 \times 10^1$	1×10^1; 1.1×10^1; 2×10^1; 1.08×10^2	1,2,3,4
$K_{S,EA}$ (nitrate)	[M]	$8.18 \times 10^{-6} \pm 4.84 \times 10^{-6}$	1.6×10^{-6}; 3.2×10^{-6}; 1.2×10^{-5}; 1.8×10^{-4}	1,3,2,4
$K_{S,ED}$ (ethanol)	[M]	$1.18 \times 10^{-4} \pm 4.55 \times 10^{-5}$	8.3×10^{-6}; 1.7×10^{-4}; 6.6×10^{-4}; 7.3×10^{-2}	1,2,3,4
b	$[d^{-1}]$	$1.73 \times 10^{-1} \pm 4.66 \times 10^{-2}$	6×10^{-2}; 1.5×10^{-1}; 2×10^{-1}	2,4,3

[a] References are 1, Chen and MacQuarrie (2004); 2, Lee et al., (2009); 3, Kinzelbach et al., (1991); 4, Rodríguez-Escales et al., (2014).

Table5
Click here to download Table: Table5_v2.docx

Authors	Feeding strategy	Sediment	Time of feeding strategy (d)	Biological process	Organic carbon inflow (mM C)	Velocity (m/d)	α/α_0 (observed time)
This work	Weekly	Sand (0.5-0.8 mm)	100	Denitrification using ethanol	260-235	0.5	1 (100 d)
	Daily		200		14-35		7 (200 d)
Taylor and Jaffé (1990) and Taylor et al. (1990)	Continuous	Sand	284	Methanol oxidation (aerobic conditions)	0.22	27.2	100-1000
			356		0.17	9.1	100-1000
Bielefeldt et al. (2002)	Continuous	Sand (0.32 mm)	50	Naphthalene degradation (aerobic conditions)	1.6	3.3	1.8 (25-46)
						7.5	3-4.8 (37-44)
						11.2	2.2 (32-50)
Seifert and Engesgaard (2007)	Continuous	Sand (0.4-0.8 mm)	150	Acetate oxidation (aerobic conditions)	0.15	5.1	2 (13 d)
							7 (45 d)
Delay et al. (2013)	Continuous	Coarse crushed limestone (2 cm)	1.4	Denitrification using ethanol	1.52	34.6	1 (1.4 d)
					2.23	138.2	1 (1.4 d)